Joint recovery of graphite and lithium metal oxides from spent lithium-ion batteries using froth flotation and investigation on process water re-use

Salces, A. M.; Bremerstein, I.; Rudolph, M.; Vanderbruggen, A.;

Originally published:

June 2022

Minerals Engineering 184(2022), 107670

DOI: https://doi.org/10.1016/j.mineng.2022.107670

Joint recovery of graphite and lithium metal oxides from spent lithium-ion batteries using froth flotation and investigation on process water re-use

Aliza Salces[1], Irina Bremerstein[2], Martin Rudolph[1], Anna Vanderbruggen[1,3]

[1] Helmholtz Zentrum Dresden Rossendorf (HZDR), Helmholtz Institute Freiberg for Resource Technology (HIF), Chemnitzer Straße 40, 09599 Freiberg, Germany

[2] UVR-FIA GmbH, Chemnitzer Straße 40, 09599 Freiberg, Germany

[3] Department of Chemical and Metallurgical Engineering, School of Chemical Engineering, Aalto University, P.O. Box 16200, 00076 Aalto, Finland

* Corresponding author. Email address: a.salces@hzdr.de

Highlights

- Graphite recovery of 85% in the overflow product in a single-stage rougher flotation.
- Lithium metal oxides recovery of 80% in the underflow product.
- Lithium accumulates in high concentrations up to 2,600 mg/L after three water cycles.
- Ease of lithium mobilization from spent Li-ion battery, particularly when subjected to thermal treatment such as pyrolysis.
- Flotation with Li-rich water does not significantly impact the flotation efficiency; hence water recirculation is viable.

Graphical abstract

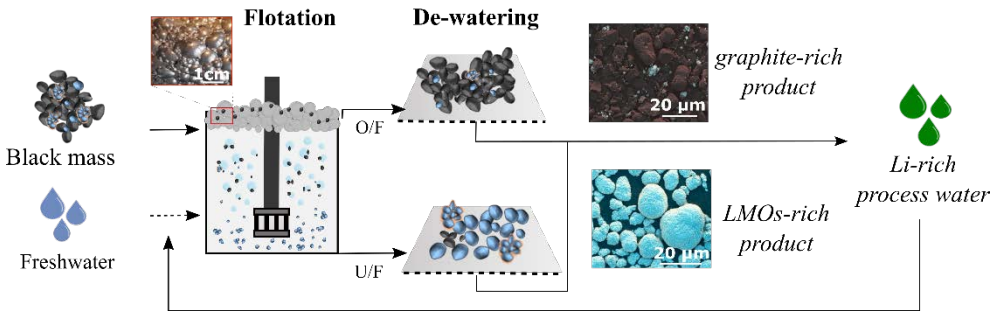

Abstract

Spent lithium-ion batteries (LIBs) contain critical raw materials that need to be recovered and recirculated into the battery supply chain. This work proposes the joint recovery of graphite and lithium metal oxides (LMOs) from pyrolyzed black mass of spent LIBs using froth flotation. Since flotation is a water-intensive process, the quality of the aqueous phase directly impacts its performance. In pursuit of an improved water-management strategy, the effect of process water recirculation on black mass flotation is also investigated. The fine fraction (<100 µm) of the black mass from pyrolyzed and crushed spent LIBs was used. After flotation, 85% of the graphite in the overflow product and 80% of the LMOs in the underflow product are recovered. After flotation with 8 wt.% solids, the process water contains about 1,000 mg/L Li and accumulates up to 2,600 mg/L Li after three cycles. The flotation with process water shows no significant impact on the recovery and grade of flotation products, suggesting the feasibility of water recirculation in black mass flotation.

Keywords: black mass, lithium-ion batteries, lithium metal oxide, spheroidized graphite, recycling, froth flotation, water recirculation

1. Introduction

Lithium-ion batteries (LIBs) are the fastest growing technology in the market as transport electrification becomes the immediate action to attain the Paris Agreement target of a well-below 2ºC global temperature rise. By 2030, it is estimated that 34 million electric vehicles (EVs) will be sold with batteries weighing between 200 - 500 kg depending on the type of EVs (Global Battery Alliance, 2019; Ellingsen et al., 2016). These batteries have a projected service life of only 10-15 years (NEDO, 2017; EUCAR, 2019) which will result in the accumulation of waste LIBs. Hence, issues regarding the massive increase in raw battery material demand

and waste management are expected to arise. The combination of mining and recycling will be essential and unavoidable to meet the upcoming demand for LIBs and to handle the hazardous LIBs waste. Recycling will also ensure the leverage of battery use, considering that mining of battery material is the major contributor to its environmental impacts (Dai et al., 2019). In Europe, the battery regulation is pushing a recovery target of 95% for cobalt, copper, and nickel, and 70% for lithium by 2030. Mandatory recycled content of 12% Co, 4% Li, and 4% Ni will also be imposed in the production of industrial, EV, and automotive batteries (Halleux, 2021).

The current battery recycling initiatives mainly aim to recover high-valued metals (e.g., Co, Ni, and Cu) by pyrometallurgy, hydrometallurgy, or their combination (Velázquez-Martínez et al., 2019). Direct recycling, which preserves the functional integrity of electrode material, is also proposed as a cost-efficient process to recover LMOs (Chen et al., 2016; Gaines et al., 2021; Sloop et al., 2020), particularly for $LiFePO_4$ and $LMnO_2$ due to their low economic value. Graphite, which comprises 15-20% of the battery's weight (Gaines et al., 2011) and ~30%-40% of battery's fine fraction (<100 µm) (Vanderbruggen et al., 2021a), is not prioritized in current recycling processes but will become crucial in attaining the recycling targets. The new EU battery regulatory framework will increase the material recovery from 50% to 65% by 2025 and 70% by 2030 (Halleux, 2021). To increase material recovery in LIB recycling processes, mechanical sorting (i.e., shredding and sieving) is indispensable to separate LIB components before their downstream processing. This step yield into two fractions: a coarse fraction containing the electrode foils and a fine fraction called "black mass" containing the active electrode material. The coarse fraction can be processed mechanically (e.g., air classification, gravity concentration, or magnetic separation) to separate plastic or metal casing, separator, and electrode foils (Werner et al., 2020). Hydrometallurgy is the preferred stage for separating and recovering black mass components by dissolving the LMOs with organic or inorganic acids and

filtering graphite at the end of the process (Or et al., 2020). However, during leaching, graphite adds volume to the feed material resulting in higher water and reagent consumption and challenges in the dewatering stage (Porvali et al., 2019; Vanderbruggen et al., 2022). Graphite may also be damaged during the metal leaching, resulting in unsuitability for upcycling spent anode materials (Zhan et al., 2021).

Froth flotation, a separation process based on the difference of surface wettabilities, is seen as a potential solution to separate the anode graphite and LMOs before the downstream processing (He et al., 2017; Kim et al., 2003; J. Yu et al., 2018; Zhan et al., 2018; Zhang et al., 2019). Graphite and LMOs have contrasting surface wettabilities, but their efficient separation is impeded by a binder coating which induces a similar wettability to graphite and LMOs (Vanderbruggen et al., 2021b; J. Yu et al., 2018; Zhan et al., 2018; He et al., 2017; Kim et al., 2003). Several pre-treatments to remove the binder and improve the flotation performance were investigated. These include chemical dissolution with Fenton reagent (He et al., 2017; Yu et al., 2017; Qiu et al., 2022) mechanically-induced stress such as mechanical grinding (Yu et al., 2018), cryogenic grinding (Liu et al., 2020), ultrahigh shear forces (Shin et al., 2020; Zhan et al., 2020) and thermal treatment (Kim et al., 2003; Wang et al., 2018; Zhan et al., 2021; Zhang, et al., 2019; Vanderbruggen et al., 2022)

The chemical dissolution with Fenton ((Fe^{2+}/H_2O_2) reagent resulted to a concentrate grade of ~55% LCO (calculated from its Co content of 39.91 wt %) with a recovery of 98.99% (He et al., 2017). Yu et al. (2017) proposed an improved Fenton flotation by controlling the $Fe(OH)_3$ precipitation with HCl which increased the concentrate grade to 75% LCO. Mechanical grinding resulted to a concentrate grade of 97.1% LCO but only a recovery of 49.3% (Yu et al., 2018). Cryogenic grinding at -196°C resulted in an improved concentrate grade up to 91.75% LCO with a recovery of 89.83% (Liu et al., 2020). The application of ultrahigh shear

forces using a high-shear blender yielded to a concentrate grade of 90.0% LCO with a total recovery of 66.0% (Shin et al., 2020). Despite these good results, these techniques were limited to lab-scale application due to difficulties in up-scalability. Also, the mechanical grinding process breaks the spheroidized anode graphite hindering its direct use in battery application.

Thermal treatment at 400°C to 600°C in a vacuum, inert gas, or air is the prevalent technique investigated due to its effectivity and ease of upscale to industry application (Kim et al., 2004; Zhang et al., 2018; Zhang et al., 2019; Zhan et al., 2021; Vanderbruggen et al., 2022). These previous research reported high LMOs recovery in the cell product of between 80% and 98%, and graphite recovery in the froth product of around 95-98%.

In several published flotation studies, the LIBs were either manually dismantled to obtain the individual components or directly crushed and sieved to get the mixed black mass before various binder-removal techniques. In this work, intact automotive cells were pyrolyzed under N_2 gas before shredding. The pyrolysis pre-treatment enabled the removal of binder and delamination of active components from metal foils, thus shortening the processing steps; however, the formation of complex compounds or binder residuals can occur and deposit on the particles' surface. Attrition and ultrasonic cleaning have been suggested to clean and refresh the particle surfaces from residual binders and pyrolysis by-products (Zhang et al., 2018; Vanderbruggen et al., 2022). To improve the flotation selectivity, attrition pre-treatment is also implemented in this work.

The novelty of this work is the focus on the process water of black mass flotation and the prospect of its re-use. Indeed, flotation is a water-intensive process. Water re-use has been an increasing practice in mineral processing due to pressure from the local government, freshwater availability, and effluent volume minimization (Rao & Finch, 1989). However, water re-use results in the accumulation of ions and flotation reagents which changes the flotation system

generating a positive or negative impact on its efficiency (Rao & Finch, 1989). For instance, certain inorganic salts (e.g., Na_2SO_4, $MgCl_2$, NaCl, $CaCl_2$, $MgSO_4$, $Al_2(SO_4)_3$, and Na_3PO_4) were reported to inhibit bubble coalescence, which influences the bubble size, gas hold-up, froth stability, and therefore recovery by entrainment (Craig, 2004; Keitel & Onken, 1982; Zieminski & Whittemore, 1971). In coal flotation, increased concentration of hydroxide forming cations such as Ca^{2+}, Fe^{2+}, Fe^{3+}, Al^{3+}, that form a passive film on particles surfaces can lead to depression of coal (Celik & Somasundaran, 1986). Similar effects can be expected in the flotation of flake graphite which could be extrapolated to anode graphite. However, most of the knowledge on process water chemistry is related to primary resources and none on secondary resources like black mass.

The black mass system is a complex containing: organics, metals and electrolyte. These components can mobilize into the water. The electrolyte salt in the liquid phase can bring Li, F, and P into the process water. The fine powders of the active electrode materials is also susceptible to dissolution in water (Zhang et al., 2013). After a thermal treatment, Li from cathode active materials has been reported to selectively dissolve in water (Li et al., 2016; Xiao et al., 2017; Balachandran et al., 2021; Zhang et al., 2022). Also, flotation reagents such as hydrocarbon oils (e.g., kerosene, diesel) used in black mass flotation are likely to remain dispersed in the process water. Still, their effects on the process remain unknown. This work investigates the process water of black mass flotation for the first time. The flotation water is used up to three cycles to determine the extent of ion accumulation and the effect of residual reagents on flotation efficiency. Ultimately, this work envisages a water management strategy in black mass flotation.

2. Material and Methods

2.1. Fine fraction of the spent black mass as flotation feed

An industrial scale operator provided the pyrolyzed black mass from automotive cells. The automotive cells underwent pyrolysis at 500°C for 1 hour under N_2 gas and shredded. A two-stage dry sieving was performed using 1-mm and 90-µm screen to obtain the black mass powder. The pyrolyzed black mass was then split into homogenous batches using a riffle splitter for the flotation test.

The black mass showed d_{50} of 11.1 µm and d_{90} of 29.6 µm, obtained by laser diffraction (HELOS, Sympatec GmbH, Clausthal-Zellerfeld, Germany). Its elemental composition (in Fig. 1) was acquired by x-ray fluorescence (XRF), inductively coupled plasma - optical emission spectrometry (ICP-OES), and carbon analysis. The black mass contains mainly liberated active particles, resulting in a low Al (2.5%) and Cu (0.2%) foils. The higher concentration of Al than Cu is linked to the induced brittleness and oxidation of Al caused by pyrolysis (Vanderbruggen et al., 2021a; Li et al., 2019; Sun & Qiu, 2011;). It has a total carbon content of 43.8%, encompassing the graphite, carbon black, and residual binder material. It also contains 3.9% Li, originating from the LMOs and electrolyte salt. The LMOs are mainly NMC cathode-type composed of 14.6% Co, 12.7% Mn, and 12.1% Ni. Additionally, black mass contains 0.9% F and 1.0% P, possibly in the form of complex compounds from the decomposition of polymeric binder and electrolyte salt.

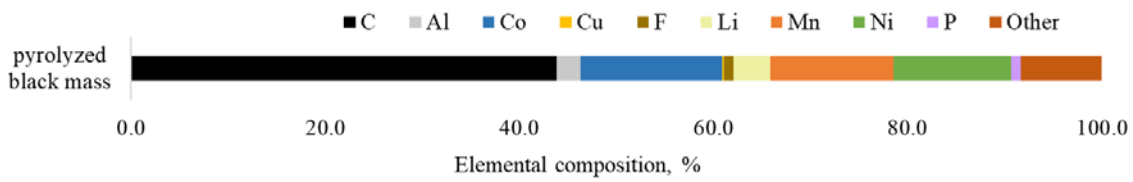

Figure 1. Elemental composition of BM obtained with XRF. Light elements such as Li, F, and C were measured by ICP-OES, IC, and carbon analysis, respectively.

In addition, a model black mass was used to check the dissolution of Li from LMOs. The model black mass was prepared by mixing Nickel-Manganese-Cobalt oxides (NMC-111 from MSE supplies, product No. PO0126) and natural spheroidized graphite (from ProGraphite GmbH, product No. 1112-1) at a ratio of 60:40.

2.2. Froth flotation

The batch flotation tests were conducted in a laboratory-scale mechanically stirred cell GTK Labcell from Outotec with automatic scraping, using a 2 L capacity cell. Fig. 2 shows the schematic flowsheet of the flotation experiment performed at fixed parameters with an impeller speed of 1000 rpm, air flowrate of 5 L/min, and scraping frequency of 6 s. For attrition, a dispersing instrument (T25, IKA ULTRA-TURRAX®) was utilized at an agitation speed of 16,000 rpm for 10 mins. The pulp density was set to 20 wt.% solids for experiments with attrition pretreatment and diluted to 8 wt.% solids afterward. Methyl isobutyl carbinol (99% $C_6H_{14}O$, Product No. A13435, Alfa Aesar) was used as frother with a dosage of 250 g/t. A 100-mL emulsion of 250 g/t of diesel and 250 g/t Ekofol 440 (EKOF Mining & Water Solution GmbH) was used to enhance the hydrophobicity of spent graphite. Five overflow products were collected for 15 mins (O/F 1 - 0.5 min, O/F 2 - 0.5 min, O/F 3 - 1 min, O/F 4 - 3 mins, O/F 5 - 10 mins). After each flotation experiment, the mass of collected froth was measured before and after drying in an oven under natural convection for 12 h at 45°C to determine mass and water pull. Finally, representative samples of the overflow product were analyzed to obtain the elemental content. The flotation recoveries were calculated using Equation (1), where *C* is the mass of the concentrate, *c(i)* is the content of material *i* in the concentrate, *F* is the mass of the feed, and *f(i)* is the grade of material in feed.

$$R(i) = \frac{C.c(i)}{F.f(i)} \quad (1)$$

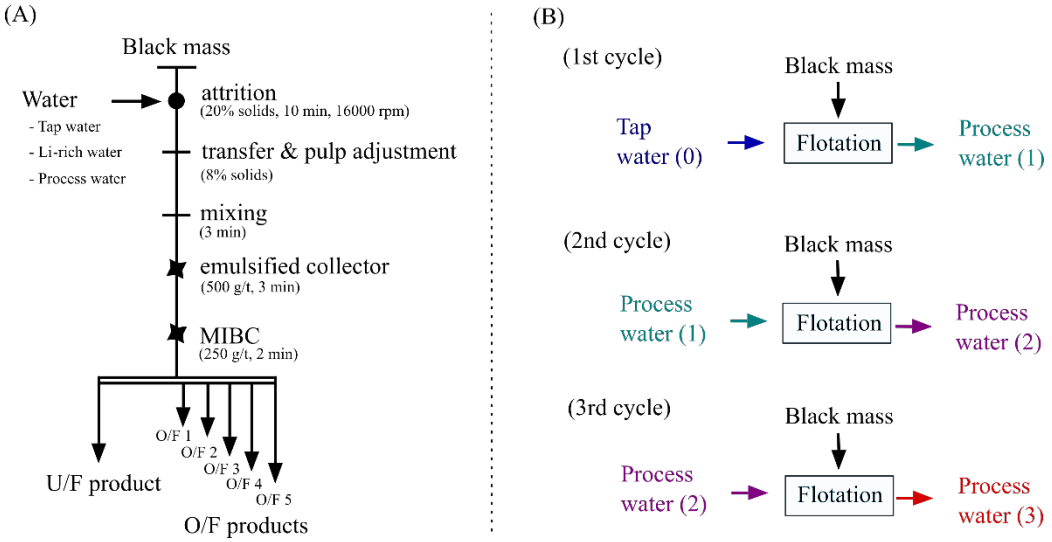

Figure 2. (A) Schematic flowsheet of the flotation experiment and (B) water flow for the process water. U/F: underflow, O/F: overflow.

2.3. Flotation waters

Three types of water were used in the flotation experiments: tap water, synthetic lithium-rich water, and process water. Fig. 3 compares the concentration of selected ions in the flotation waters tested.

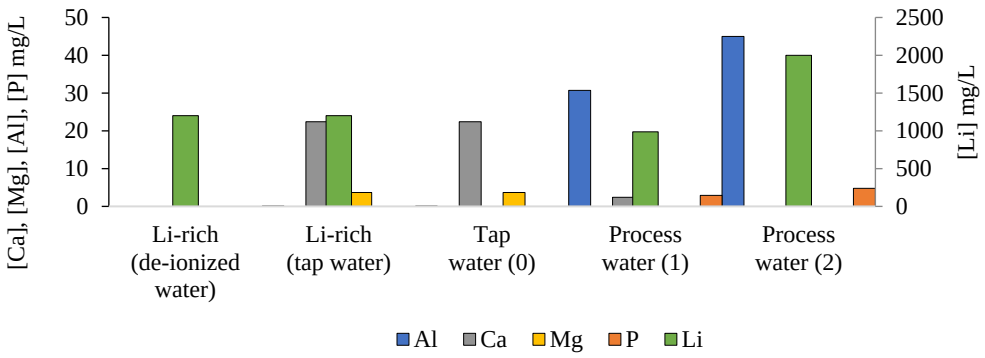

Figure 3. Concentrations of selected cations in the flotation water.

The tap water (0) was sourced from the Helmholtz Institute of Freiberg (HIF) water supply. Ten tap water samples were collected in one month to check the ion content variability. On

average, the tap water (0) contained 22.4±0.6 mg/L Ca and 3.7±0.2 mg/L Mg, 0.2±0.1 mg/L Al and average pH of 8.3±0.1. The synthetic Li-rich water was made from mixing 99.9% Li_2CO_3 powder (99% ACS reagent, Sigma-Aldrich) with tap water or de-ionized water. Both have a Li concentration of ~1200 mg/L and a pH of 11.4.

After the flotation tests, the water for the second and third cycle was collected by a filtration process, as shown in Fig. 2B. On average, the process water (1) contained 980 mg/L Li, 30 mg/L Al, and 2 mg/L Ca, while Mg is below the detection limit. Process water (2) contained 2000 mg/L Li and 45 mg/L Al, while Ca and Mg were below the detection limit. The average pH of both process water is 11.3 ± 0.1.

In addition, the stability of ions in the process water was verified. After one-month of storage, no changes in Li concentration were observed, while Mg, Ca, Al, and P concentration decreased.

2.4. Analytical methods

The flotation samples were analyzed using an XRF (NitonTM XL3t 980, Thermo Scientific) for their metal content. The carbon content was commissioned to the EUROFINS laboratory (Freiberg, Germany). The total carbon content (TOC) determination procedure consists of high-temperature combustion (1200 ºC) followed by infrared spectroscopy analysis of the derived CO_2 gas. The lithium content of the flotation feed and products was determined through acid digestion. A 200-mg solid sample was reacted with 15 mL nitric acid (67-69% HNO_3, Suprapur®) and 10 mL hydrogen peroxide (30 wt.% H_2O_2, Arcos Organics) for two hours under constant stirring. The digested material was diluted to 100-ml using a volumetric flask and centrifuged (Centrifuge 5804, Eppendorf) to remove any solid constituents. The obtained solution was measured using ICP-OES (PQ9000, Analytik Jena).

The ion content of the water supply and processed waters was also analyzed using ICP-OES. A 25-mL representative water sample was collected and acidified with HNO3 to pH <2 for the analysis.

3. Results and discussion

3.1. Flotation efficiency

As shown in Fig 5, the flotation of pyrolyzed black mass without attrition pre-treatment resulted in a recovery of 91% graphite and 31% nickel-manganese-cobalt (Ni-Mn-Co) in the overflow product. The relatively high metal recovery in the overflow product suggests the ineffective separation between graphite and LMOs. A scanning electron microscopy (SEM) image in Fig. 4 reveals residual binder on LMOs surface even after pyrolysis, which induces hydrophobicity and the eventual collection in the overflow product. The presence of binder on LMOs particles after pyrolysis is unexpected as it is reported to decompose at 400-600°C (Sun & Qiu, 2011; Kuila et al., 2015; Zhang et al., 2018; Li et al., 2019; S. Yu et al., 2020). Binder residuals were also observed by Vanderbruggen et al. (2022) after pyrolysis of the black mass sample. For this material, this can be due to the thermal gradient inside the unopened automotive cell during pyrolysis. Hence, second pyrolysis was performed at 550 °C for two hours, however, LMOs aggregation was still observed, raising the question of whether the above-mentioned temperature range is sufficient for complete binder decomposition. With the persistence of residual binder, attrition pre-treatment was implemented to potentially refresh the LMOs surface and improve flotation efficiency (Vanderbruggen et al., 2022).

With attrition, a noticeable improvement in flotation efficiency is demonstrated in the grade-recovery curve in Fig. 5. In the overflow product, graphite grade increased from 66% to 79% C, and NMC grade decreased from 27% to 16%. A slight decrease in graphite recovery from

91% to 85% could be attributed to its slower flotation kinetics with attrition as evident in the marked difference between their recoveries after 5-min and 15-min of flotation (Fig. 6A). Nevertheless, a similar recovery about 90% graphite was achieved in an extended of flotation time (i.e., in a 5-min scavenging). The slow flotation kinetics of graphite is inferred due to an occurrence of partial slime coating as attritioning generates ultra-fine particles that may have incompletely passivated its surfaces.

Furthermore, the surface condition of spent graphite (Fig. 4) impacts its floatability. Zhan et al. (2021) reported an oxygen-rich hydrophilic layer associated with solid electrolyte interface (SEI) on the surface of age anode material which affects its flotation. To verify this, a model black mass containing fresh graphite and LMO was used in flotation. Fig. 6A revealed a faster flotation of fresh graphite in which 80% is recovered after 1-min and 95% after 5-min flotation compared to 24% and 67% recovery after 1-min and 5-min, respectively, of graphite in the spent black mass. These results emphasize the contamination of graphite surface during the LIBs use and recycling process, which becomes a significant consideration in flotation.

The shift in the upgrading curve in Fig. 5C shows the improvement of efficiency after attrition pre-treatment. Indeed, attrition refreshes LMOs surface by removing a part of residual binder, thereby reducing its true flotation. Equally, it disperses the black mass particles, reducing metals' entrapment in unselective agglomerates (Vanderbruggen et al., 2022).

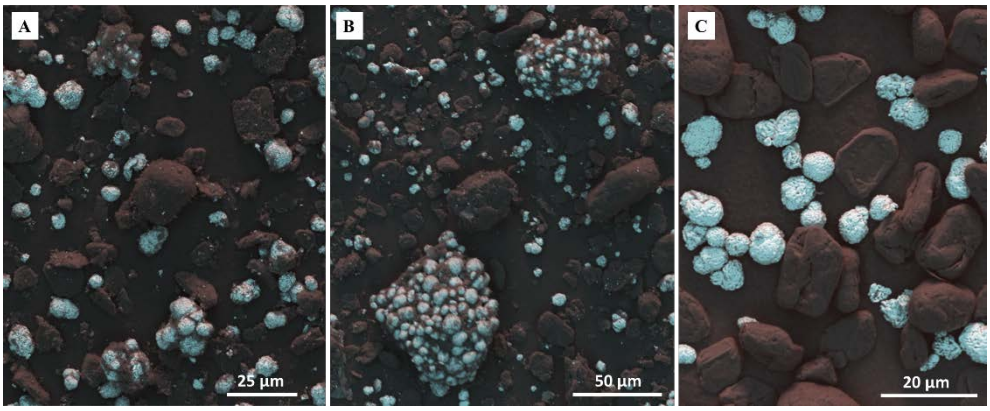

Figure 4. SEM image with imposed colors of graphite (black) and LMOs (blue). (A) pyrolyzed spent black mass (B) pyrolyzed spent black mass after second thermal treatment showed LMOs aggregated with binder (C) model black mass containing pristine materials (binder-free).

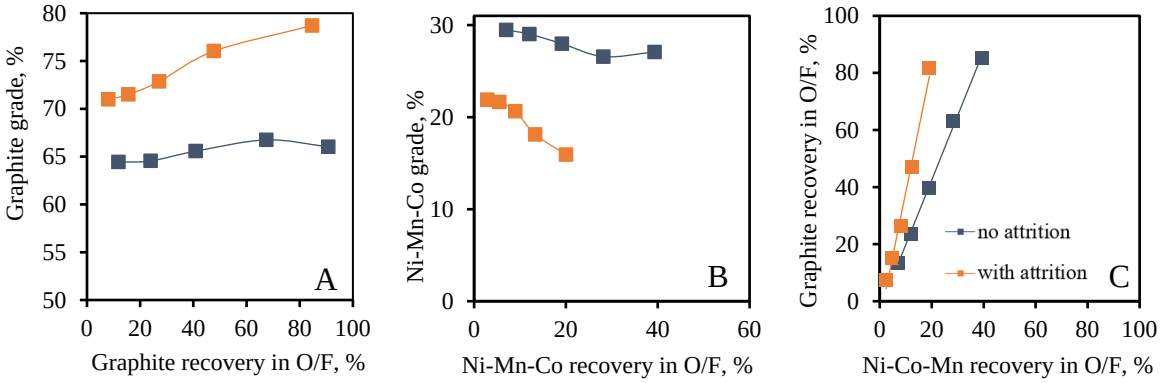

Figur e 5. The grade-recovery curve of (A) graphite and (B) NMC, and (C) their upgrading curve.

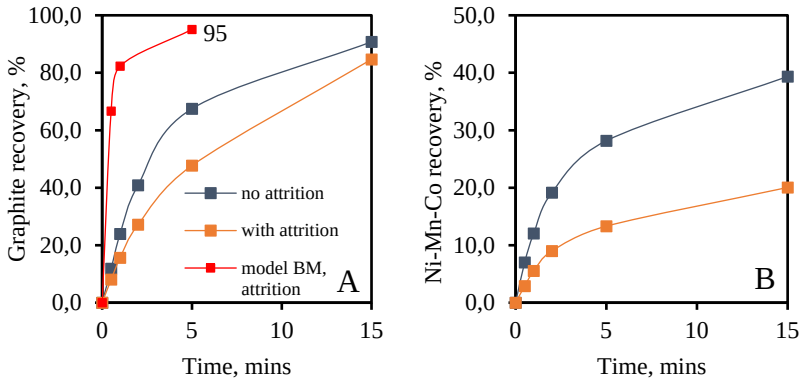

Figure 6. Flotation kinetics of (a) graphite and (b) Ni-Mn-Co. Flotation kinetics of graphite in model BM (in red) included for comparison.

3.2. Dissolution of black mass components in flotation water

Spent LIBs contain various elements in the solid and liquid (electrolyte) phases that may mobilize when in contact and immerse in water. Fig. 7 shows the ion concentrations in flotation water after successive water utilization and Table 1 summarizes the possible origin of these ions.

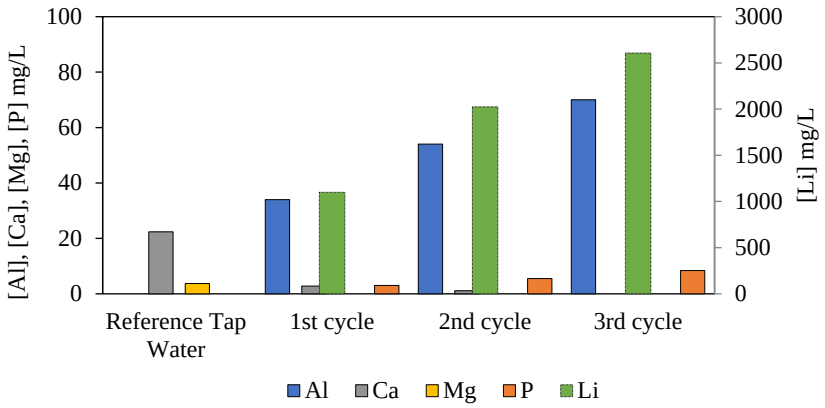

Figure 7. Ion concentration after each flotation.

Table 1. Possible origins of ions in the flotation process water. NCA and LFP are not present in the studied black mass.

Ions	Possible origins
Al	Al foils
Ca	Calcite fillers in housing plastics, tap water
F	Electrolyte (LiFP6), Polyvinylidene fluoride binder (PVDF)
P	Electrolyte (LiFP6), *lithium iron phosphate (LFP)*
Li	LMOs, electrolyte (LiFP6), spent anode graphite + SEI

Sample	Origin of lithium
spent black mass	LMOs, electrolyte ($LiFP_6$), spent anode graphite
model black mass	LMOs
fresh pyrolyzed model black mass	LMOs
fresh battery	LMOs, electrolyte

The Al concentration increased from below <0.1 mg/L to about 34 mg/L, 54 mg/L, and 70 mg/L after the subsequent water use. The Al ions in this black mass sample originate from the cathode foil. However, Al could also be contributed by an NCA cathode-type but is not present in this sample. The P concentration also increased from below <0.1 mg/L to about 3.0 mg/L, 5.8 mg/L,

and 8.4 mg/L. In this study, the source of P is the electrolyte salt, in other black mass samples, it could also come from the cathode active material of LFP battery. The fluorine content was only measured during the first cycle with 213 mg/L but, it is also expected to accumulate. As a waste water, this exceeds the fluorine limit required if at the point of discharge in such as the 30 mg/L F limit in Germany (Federal Law Gazette I p. 1106). The F is contributed by the electrolyte salt and PVDF binder. Its impact on the flotation system has not been investigated so far, but it will be further studied due to its possible toxicity and criticality.

Meanwhile, a decrease in Ca from 22.44 mg/L and Mg from 3.7 mg/L to <0.1 mg/L concentrations were observed and were related to the precipitation of Mg and Ca carbonates at the flotation pH of 11.3. It is also likely that Ca reacted with F to form CaF_2, to which a Ca-rich was found during SEM analysis (Fig. S1 in Supplementary material). Hence, the introduction of Ca in the flotation system could be a solution to reduce the F ions in the process water.

Among the ions in the process water, the Li concentration significantly increases to ~1100 mg/L, ~2020 mg/L, and ~2,600 mg/L after the 1^{st}, 2^{nd}, and 3^{rd} cycle. These correspond to Li dissolutions of around 45%, 43%, and 25%, respectively after each cycle, from the original Li content of spent black mass. The high dissolution of Li could be related to the formation of water-soluble Li compound in the carbothermic reduction of LMOs during pyrolysis, as explained by Li et al., (2016) and Lombardo et al. (2019). However, the extent of Li dissolution is surprisingly high considering that the black mass powder is stirred in water for only 23 mins at an average temp ~23ºC. The high temperature (max 38 ºC) during 10-min attrition did not result in appreciable Li dissolution variation with only about 1% difference. The selective water leaching of Li from pyrolyzed LMOs has been reported in several researches (Li et al., 2016; Xiao et al., 2017; Balachandran et al., 2021; Zhang et al., 2022).

It is also notable to mention the sudden decrease in Li dissolution after third water re-use, which may suggest that maximum solubility of the Li compound in pyrolyzed spent black mass is exceeded. Lithium oxide (Li_2O) and lithium carbonate (Li_2CO_3) were among the reported products of carbothermic reduction of LMOs in a study by Lombardo et al, (2019, 2020). Li_2O is highly reactive in water and forms lithium oxide (LiOH), with a solubility of 128 g/L (i.e., 12,000 mg/L Li) at 20 ºC. Li_2CO_3 is slightly soluble in water with only 13.0 g/L (i.e., 2,500 mg/L Li) at 20 ºC. The solubility of Li compounds is indicative of the maximum Li concentration in the process water. The first and second cycles both showed a similar Li dissolution. After the third cycle, it decreased to 25% with 2,600 mg/L Li in the process water, which can indicate that the major form of Li compound is Li_2CO_3. Consequently, the maximum Li content of the process water will be limited to the low solubility of Li_2CO_3. The solubility of Li_2CO_3 also decreases with the increase in temperature which can explain the minimal effect of attrition on the Li dissolution.

The sources of Li (Table 1) in spent black mass are cathode active materials, electrolyte salt, and even the anode graphite. According to Gaines et al. (2021), the anode graphite at the end of life of the battery can contain at least 16% Li that was originally from the cathode active materials. In the 150 g flotation feed, 5.8 g are estimated to be Li based on the sample characterization (c.f. Section 2.1) and of which 2.5 g dissolved into the process water. To check the source of Li and its dissolution, a model black mass consisting of only pristine LMOs and graphite without electrolyte was prepared. After a similar flotation procedure, only 0.2% Li from the LMOs dissolves in water. Since pyrolysis is reported to produce water-soluble Li compound, the same MBM was thermal treatment at 550°C for 2 h, but only 2.7% of Li was dissolved.

In addition, a 43-g cylindrical NMC type battery (INR18650M29, Samsung) was used to estimate the content of Li in the electrolyte. The battery was opened, unrolled, and immersed in 2 L de-ionized water for an hour. A mass loss of 11.6% was recorded and attributed to the electrolyte liquid which is in agreement with Gaines et al. (2011) and of which 2.4% is Li (~0.12 g). These values are minor compared to ~45% Li dissolution in spent black mass, suggesting that Li from the uncycled cathode is not easily mobilized. Consequently, these imply the ease of Li mobilization from spent LIBs, particularly if subjected to high heat treatment such as pyrolysis, generating actions on future water management in LIBs recycling processes and awareness of lithium loss in the cathode active material in case of direct recycling process. Moreover, such enriched water can be a viable source of Li comparable to salt brines as primary Li resources. In fact, the process water, which can contain up to 2,600 mg/L Li, has higher Li content than Salar del Hombre Muerto of Argenta (600 mg/L) and Salar de Atacama of Chile (~1500 mg/L) (Tabelin et al., 2021) proving the importance of its recovery.

3.2.1 Effect of Li in flotation

The high concentration of ions in the process water can positively or negatively affect the flotation efficiency as relatively small, and the multivalent ions like Li^{+}, Na^{+}, Ca^{2+}, Mg^{2+}, $A1^{3+}$ and highly charged ions such as SO_4^{2-} and PO_4^{3-} were reported to increase the water viscosity (Zieminski & Whittemore, 1971; Kavanau, 1964). The water viscosity affects the degree of bubble coalescence and affects the froth stability, water drainage, and recovery by water entrainment. Accordingly, Zieminski & Whittemore (1971) reported Li^{+} exhibits an effect on the degree of coalescence due to *"its a small radius which allows it to approach a water molecule more closely, polarize it, thus strengthening the electrostatic bonds between the water molecules"*.

To determine the effect of high Li concentration, synthetic Li-rich de-ionized water, and Li-rich tap water were used. Fig. 8a and 8b show the effect of high Li concentration on the grade-recovery curve of graphite and Ni-Mn-Co. With Li-rich waters, similar graphite recoveries (~85%) were noted, however a decrease in graphite grade is visible due to slightly higher Ni-Mn-Co recovery (~1-2%) in the overflow product. While it is mentioned that Ni-Mn-Co recovery is mainly due to true flotation imparted by its binder coating, recovery due to water entrainment also plays a critical contribution. In Fig. 9, the water recovery is found to increase with the increase of ions in the water (Li-rich tap water > Li-rich de-ionized water >> tap water), a phenomenon also documented in several works, which is attributed to the increase in froth stability (Dzingai et al., 2020; Manono et al., 2019; Biçak et al., 2012). A linear correlation is evident between the Ni-Mn-Co and water recovery (Fig. 9A) while graphite recovery remains unaffected (Fig. 9B). Despite no perceptible froth changes, it is theorized that the presence of Li ions contributes to froth stabilization leading to less water drainage and slightly higher water recovery, in turn increasing Ni-Mn-Co recovery by entrainment. However, without a drastic effect on graphite and Ni-Mn-Co recovery, it is concluded that a high Li concentration does not affect the flotation performance, or at least in the concentration tested.

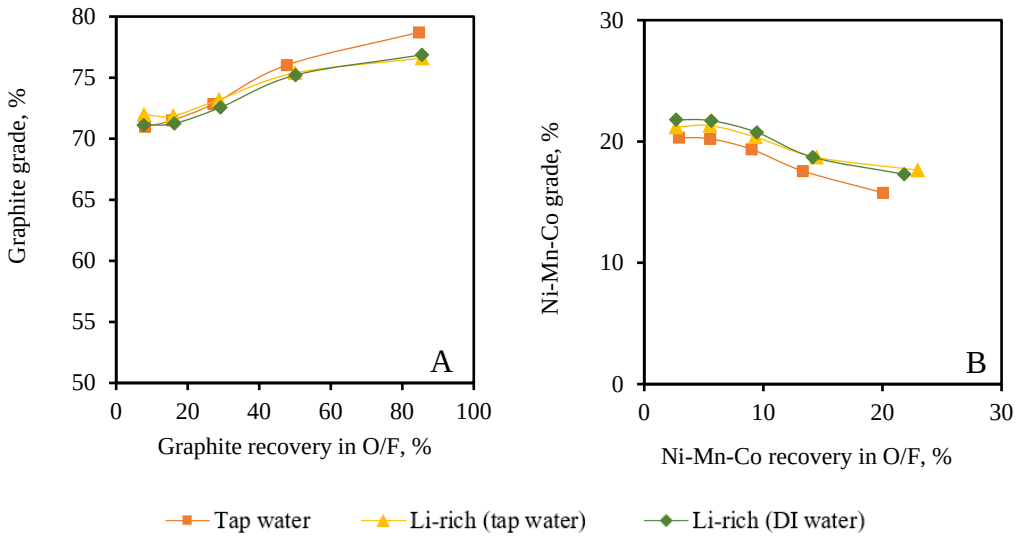

Figure 8. The grade-recovery curve of (a) graphite and (b) Ni-Mn-Co in the overflow product.

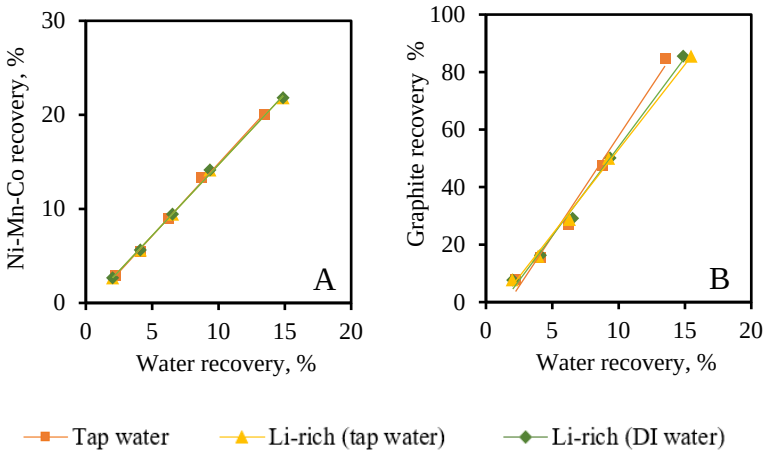

Figure 9. Ni-Mn-Co and graphite recovery vs. water recovery.

3.2.2 Water recirculation

Based on the results above (Section 3.2.1), the feasibility of flotation water recirculation is investigated up to three water cycles. Fig. 10a and 10b shows the grade-recovery curve of graphite and Ni-Mn-Co after each water re-use. A slight decrease in graphite recovery of ~5% is recorded after each water cycle (i.e., 85%, 81%, and 76% in 1st, 2nd, and 3rd cycle respectively). Similarly, it is inferred to be related to much slower flotation kinetics, where comparable recovery is achieved after extended flotation time. The Ni-Mn-Co recovery remains around 20% despite the increase of water recovery from 13%, 15%, and 16% after 1st , 2nd , and 3rd cycle respectively.

It is also important to emphasize that residual reagents such as MIBC, Ekofol, and diesel might be present in flotation water, which is the same flotation water used during attrition pre-treatment. According to Vanderbruggen et al., (2022), an addition of non-selective hydrocarbon collector (e.g., kerosene, diesel) during the attrition pre-treatment results to higher recovery of LMOs in the overflow product due to increased collision probability between LMOs particles

and oil droplets. This is not observed during water re-use which can indicate minimal content of hydrocarbon reagent in the process water. The hydrocarbon reagents are likely to mainly adsorb on the graphite surfaces which reports in the overflow product. Therefore, these results underline the non-significant impact of subsequent water recirculation on flotation efficiency or at least in the concentration of ions tested.

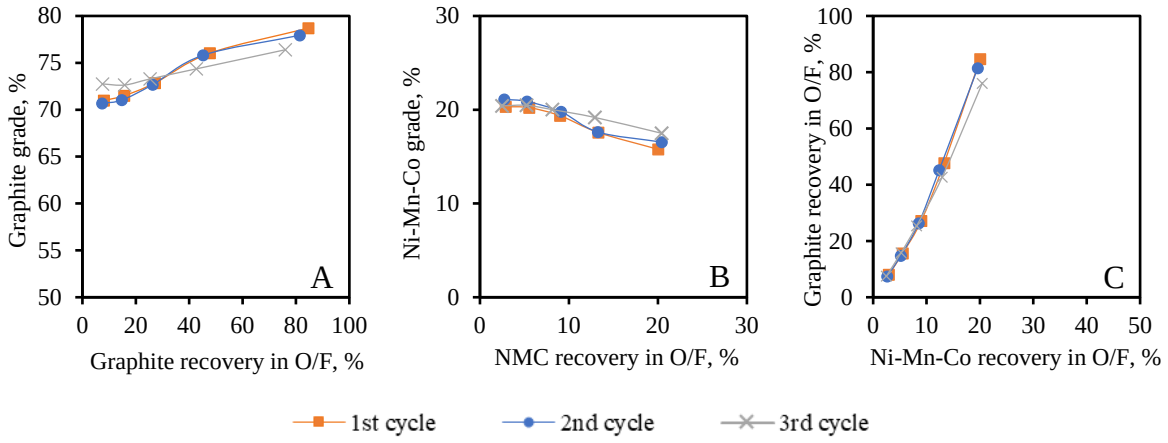

Figure 10. The grade-recovery curve of (a) graphite and (b) Ni-Mn-Co, and (c) their upgrading curve.

4. Conclusion and outlooks

This work demonstrates that a separation of graphite in the overflow product and lithium metal oxides in the underflow product, from industrially pyrolyzed black mass can be achieved through froth flotation. The application of attrition pre-treatment enhanced the flotation selectivity, resulting in an increase in LMOs recovery in the underflow product from 60% to 80%. The process water characterization reveals a Li accumulation of up to 2,600 mg/L after three cycles of water use. It is hypothesized that Li is mainly derived from the electrolyte salt and LMOs, which can be in their original form or chemically altered during battery use and after recycling pre-treatments such as pyrolysis. In addition, it is essential to highlight that a high concentration of F^- in the process water is found up to 200 mg/L and is expected to increase with further water recycling. The flotation in Li-rich process water does not show a substantial

impact on its efficiency which resulted in comparable grade and recovery of graphite and LMOs as compared to the case when fresh water is used. This highlights the feasibility of water re-use. However, it is also relevant for upcoming studies to investigate the saturated water and further explore different water sources such as seawater or hard water (e.g., Ca or Mg rich).

Overall, this work resulted in the recovery of three strategic products from the flotation of black mass from spent LIBs: graphite in the overflow product, LMOs in the underflow, and Li in process water. The potential recovery of Li in the process water using purification techniques is currently studied. Still, metals recovery in the underflow product must be improved using more selective reagents and further investigation on its flotation behaviour.

Acknowledgment and funding

We would like to thank Accurec Recycling GmbH for the industrial black mass samples. Gratitude is also expressed to Stefanie Schubert for the ICP-OES analyses. We would like to thank Simon Obando Sierra and Alvaro José Rodríguez Medina for their help with the flotation tests. Furthermore, we gratefully acknowledge the EMerald master program and Helmholtz-Institut Freiberg für Ressourcentechnologie for base funding within the PoF III (project-oriented funding part III) for the BooMeRanG project.

Author Contributions

A.S: conceptualization, writing, data curation; A.V: conceptualization, methodology, reviewing, and supervision, I.B and M.R: reviewing and supervision. All authors have read and agreed to the published version of the manuscript.

Declaration of Competing Interest

The authors declare that they have no known competing financial interests or personal relationships that could have influenced the work reported in this paper.

References

Balachandran, S., Forsberg, K., Lemaître, T., Vieceli, N., Lombardo, G., & Petranikova, M. (2021). *Comparative Study for Selective Lithium Recovery via Chemical Transformations during Incineration and Dynamic*.

Biçak, Ö., Ekmekçi, Z., Can, M., & Öztürk, Y. (2012). The effect of water chemistry on froth stability and surface chemistry of the flotation of a Cu-Zn sulfide ore. *International Journal of Mineral Processing*, *102–103*, 32–37. https://doi.org/10.1016/j.minpro.2011.09.005

Castro, S., & Laskowski, J. S. (2011). Froth Flotation in Saline Water. *KONA Powder and Particle Journal*, *29*, 4–15. https://doi.org/10.14356/kona.2011005

Celik, M. S., & Somasundaran, P. (1986). The Effect of Multivalent Ions on the Flotation of Coal. *Separation Science and Technology*, *21*(4), 393–402. https://doi.org/10.1080/01496398608057170

Chen, J., Li, Q., Song, J., Song, D., Zhang, L., & Shi, X. (2016). Environmentally friendly recycling and effective repairing of cathode powders from spent LiFePO4 batteries. *Green Chemistry*, *18*(8), 2500–2506. https://doi.org/10.1039/C5GC02650D

Craig, V. S. J. (2004). Bubble coalescence and specific-ion effects. *Current Opinion in Colloid & Interface Science*, *9*, 178–184. https://doi.org/10.1016/j.cocis.2004.06.002

Dai, Q., Kelly, J. C., Gaines, L., & Wang, M. (2019). Life Cycle Analysis of Lithium-Ion Batteries for Automotive Applications. In *Batteries* (Vol. 5, Issue 2). https://doi.org/10.3390/batteries5020048

Dzingai, M., Manono, M., & Corin, K. (2020). Simulating the Eff ect of Water Recirculation on Flotation through Ion-Spiking : Effect of Ca2+ and Mg2+. *Minerals*, *10*, 1033. https://doi.org/10.3390/min10111033

Ellingsen, L. A. W., Singh, B., & Strømman, A. H. (2016). The size and range effect: Life-cycle greenhouse gas emissions of electric vehicles. *Environmental Research Letters*, *11*, 054010.

Gaines, L., Sullivan, J., & Burnham, A. (2011). Paper No. 11-3891 Life-Cycle Analysis for Lithium-Ion Battery Production and Recycling. *Transportation Research Board 90th Annual Meeting, Washington, DC.*

Gaines, L., Dai, Q., Vaughey, J. T., & Gillard, S. (2021). Direct recycling R&D at the recell center. *Recycling*, *6*(2), 1–18. https://doi.org/10.3390/recycling6020031

Global Battery Alliance. (2019). *A Vision for a Sustainable Battery Value Chain in 2030 - Unlocking the Full Potential to Power Sustainable Development and Climate Change Mitigation. Report fromWorld Economic Forum.* http://www3.weforum.org/docs/WEF_A_Vision_for_a_Sustainable_Battery_Value_Chain_in_2030_Report.pdf

Halleux, V. (2021). *New EU regulatory framework for batteries - Setting sustainability requirements*.https://www.europarl.europa.eu/thinktank/en/document.html?reference=EPRS_BRI(2021)689337

He, Y., Zhang, T., Wang, F., Zhang, G., & Zhang, W. (2017). Recovery of LiCoO 2 and graphite from spent lithium-ion batteries by Fenton reagent-assisted fl otation. *Journal of Cleaner Production*, 1–7. https://doi.org/10.1016/j.jclepro.2016.12.106

He, Y., Zhang, T., Wang, F., Zhang, G., Zhang, W., & Wang, J. (2017). Recovery of LiCoO2

and graphite from spent lithium-ion batteries by Fenton reagent-assisted flotation. *Journal of Cleaner Production*, *143*, 319–325. https://doi.org/https://doi.org/10.1016/j.jclepro.2016.12.106

Keitel, G., & Onken, U. (1982). Inhibition of bubble coalescence by solutes in air/water dispersions. *Chemical Engineering Science*, *37*(11), 1635–1638. https://doi.org/https://doi.org/10.1016/0009-2509(82)80033-X

Kim, Y., Matsuda, M., Shibayama, A., & Fujita, T. (2003). Recovery of LiCoO2 from Wasted Lithium Ion Batteries by using Mineral Processing Technology. *Resources Processing*, *51*(1), 3–7. https://doi.org/10.4144/rpsj.51.3

Li, J., Wang, G., & Xu, Z. (2016). Environmentally-friendly oxygen-free roasting/wet magnetic separation technology for in situ recycling cobalt, lithium carbonate and graphite from spent LiCoO2/graphite lithium batteries. *Journal of Hazardous Materials*, *302*, 97–104. https://doi.org/10.1016/j.jhazmat.2015.09.050

Li, W., Yang, S., Liu, N., Chen, Y., Xi, Y., Li, S., Jie, Y., & Hu, F. (2019). Study on Vacuum Pyrolysis Process of Cathode Sheets from Spent Lithium-Ion Batteries. In G. Gaustad, C. Fleuriault, M. Gökelma, J. A. Howarter, R. Kirchain, K. Ma, C. Meskers, N. R. Neelameggham, E. Olivetti, A. C. Powell, F. Tesfaye, D. Verhulst, & M. Zhang (Eds.), *REWAS 2019. The Minerals, Metals & Materials Series* (pp. 421–435). Springer, Cham. https://doi.org/10.1007/978-3-030-10386-6_49

Liu, J., Wang, H., Hu, T., Bai, X., Wang, S., Xie, W., Hao, J., & He, Y. (2020). Recovery of LiCoO2 and graphite from spent lithium-ion batteries by cryogenic grinding and froth flotation. *Minerals Engineering*, *148*, 106223. https://doi.org/https://doi.org/10.1016/j.mineng.2020.106223

Lombardo, G., Ebin, B., St Foreman, M. R. J., Steenari, B. M., & Petranikova, M. (2019). Chemical Transformations in Li-Ion Battery Electrode Materials by Carbothermic Reduction. *ACS Sustainable Chemistry and Engineering*, *7*(16), 13668–13679. https://doi.org/10.1021/acssuschemeng.8b06540

Manono, M., Corin, K., & Wiese, J. (2019). The effect of the ionic strength of process water on the interaction of talc and CMC: Implications of recirculated water on floatable gangue depression. *Minerals*, *9*(4). https://doi.org/10.3390/min9040231

New Energy and Industrial Technology Development Organization (NEDO). (2017). *The Japanese policy and NEDO activity for future mobility*. https://www.nedo.go.jp/content/100873093.pdf

Or, T., Gourley, S. W. D., Kaliyappan, K., Yu, A., & Chen, Z. (2020). Recycling of mixed cathode lithium-ion batteries for electric vehicles: Current status and future outlook. *Carbon Energy*, *2*(1), 6–43. https://doi.org/10.1002/cey2.29

Porvali, A., Aaltonen, M., Ojanen, S., Velazquez-Martinez, O., Eronen, E., Liu, F., Wilson, B. P., Serna-Guerrero, R., & Lundström, M. (2019). Mechanical and hydrometallurgical processes in HCl media for the recycling of valuable metals from Li-ion battery waste. *Resources, Conservation and Recycling*, *142*(December 2018), 257–266. https://doi.org/10.1016/j.resconrec.2018.11.023

Qiu, H., Peschel, C., Winter, M., Nowak, S., Köthe, J., & Goldmann, D. (2022). Recovery of Graphite and Cathode Active Materials from Spent Lithium-Ion Batteries by Applying Two Pretreatment Methods and Flotation Combined with a Rapid Analysis Technique. *Metals*, *12*(4), 677. https://doi.org/10.3390/met12040677

Rao, S. R., & Finch, J. A. (1989). A review of water re-use in flotation. *Minerals Engineering*,

2(1), 65–85. https://doi.org/https://doi.org/10.1016/0892-6875(89)90066-6

Shin, H., Zhan, R., Dhindsa, K., Pan, L., & Han, T. (2020). Electrochemical Performance of Recycled Cathode Active Materials Using Froth Flotation-based Separation Process. *Journal of The Electrochemical Society*, *167*, 20504. https://doi.org/10.1149/1945-7111/ab6280

Sloop, S., Crandon, L., Allen, M., Koetje, K., Reed, L., Gaines, L., Sirisaksoontorn, W., & Lerner, M. (2020). A direct recycling case study from a lithium-ion battery recall. *Sustainable Materials and Technologies*, *25*, e00152. https://doi.org/10.1016/j.susmat.2020.e00152

Sun, L., & Qiu, K. (2011). Vacuum pyrolysis and hydrometallurgical process for the recovery of valuable metals from spent lithium-ion batteries. *Journal of Hazardous Materials*, *194*, 378–384. https://doi.org/https://doi.org/10.1016/j.jhazmat.2011.07.114

Tabelin, C. B., Dallas, J., Casanova, S., Pelech, T., Bournival, G., Saydam, S., & Canbulat, I. (2021). Towards a low-carbon society: A review of lithium resource availability, challenges and innovations in mining, extraction and recycling, and future perspectives. *Minerals Engineering*, *163*(July 2020). https://doi.org/10.1016/j.mineng.2020.106743

The European Council for Automotive Research and Development (EUCAR). (2019). *Battery requirements for future automotive applications* (Issue July). https://eucar.be/wp-content/uploads/2019/08/20190710-EG-BEV-FCEV-Battery-requirements-FINAL.pdf

Vanderbruggen, A., Gugala, E., Blannin, R., Bachmann, K., Serna-Guerrero, R., & Rudolph, M. (2021a). Automated mineralogy as a novel approach for the compositional and textural characterization of spent lithium-ion batteries. *Minerals Engineering*, *169*(May), 106924. https://doi.org/10.1016/j.mineng.2021.106924

Vanderbruggen, A., Sygusch, J., Rudolph, M., & Serna-Guerrero, R. (2021b). A contribution to understanding the flotation behavior of lithium metal oxides and spheroidized graphite for lithium-ion battery recycling. *Colloids and Surfaces A: Physicochemical and Engineering Aspects*, *626*, 127111. https://doi.org/https://doi.org/10.1016/j.colsurfa.2021.127111

Vanderbruggen, A., Salces, A., Ferreira, A., Rudolph, M., & Serna-Guerrero, R. (2022). Improving Separation Efficiency in End-of-Life Lithium-Ion Batteries Flotation Using Attrition Pre-Treatment. *Minerals*, *12*(1). https://doi.org/10.3390/min12010072

Velázquez-Martínez, O., Valio, J., Santasalo-Aarnio, A., Reuter, M., & Serna-Guerrero, R. (2019). A critical review of lithium-ion battery recycling processes from a circular economy perspective. *Batteries*, *5*(4), 5–7. https://doi.org/10.3390/batteries5040068

Wang, F., Zhang, T., He, Y., Zhao, Y., Wang, S., Zhang, G., Zhang, Y., & Feng, Y. (2018). Recovery of valuable materials from spent lithium-ion batteries by mechanical separation and thermal treatment. *Journal of Cleaner Production*, *185*, 646–652. https://doi.org/10.1016/j.jclepro.2018.03.069

Werner, D., Peuker, U. A., & Mütze, T. (2020). Recycling Chain for Spent Lithium-Ion Batteries. *Metals*, *10*(3). https://doi.org/10.3390/met10030316

Xiao, J., Li, J., & Xu, Z. (2017). Recycling metals from lithium ion battery by mechanical separation and vacuum metallurgy. *Journal of Hazardous Materials*, *338*, 124–131. https://doi.org/10.1016/j.jhazmat.2017.05.024

Yu, J., He, Y., Li, H., Xie, W., & Zhang, T. (2017). Effect of the secondary product of semi-solid phase Fenton on the flotability of electrode material from spent lithium-ion battery. *Powder Technology*, *315*, 139–146.

https://doi.org/https://doi.org/10.1016/j.powtec.2017.03.050

Yu, J., He, Y., Ge, Z., Li, H., Xie, W., & Wang, S. (2018). A promising physical method for recovery of LiCoO2 and graphite from spent lithium-ion batteries: Grinding flotation. *Separation and Purification Technology*, *190*, 45–52. https://doi.org/https://doi.org/10.1016/j.seppur.2017.08.049

Zhan, R., Oldenburg, Z., & Pan, L. (2018). Recovery of active cathode materials from lithium-ion batteries using froth flotation. *Sustainable Materials and Technologies*, *17*, e00062. https://doi.org/10.1016/j.susmat.2018.e00062

Zhan, R., Payne, T., Leftwich, T., Perrine, K., & Pan, L. (2020). De-agglomeration of cathode composites for direct recycling of Li-ion batteries. *Waste Management*, *105*, 39–48. https://doi.org/https://doi.org/10.1016/j.wasman.2020.01.035

Zhan, R., Yang, Z., Bloom, I., & Pan, L. (2021). Significance of a Solid Electrolyte Interphase on Separation of Anode and Cathode Materials from Spent Li-Ion Batteries by Froth Flotation. *ACS Sustainable Chemistry & Engineering*, *9*(1), 531–540. https://doi.org/10.1021/acssuschemeng.0c07965

Zhang, T., He, Y., Ge, L., Fu, R., Zhang, X., & Huang, Y. (2013). Characteristics of wet and dry crushing methods in the recycling process of spent lithium-ion batteries. *Journal of Power Sources*, *240*, 766–771. https://doi.org/10.1016/j.jpowsour.2013.05.009

Zhang, G., He, Y., Feng, Y., Wang, H., & Zhu, X. (2018). Pyrolysis-Ultrasonic-Assisted Flotation Technology for Recovering Graphite and LiCoO2 from Spent Lithium-Ion Batteries. *ACS Sustainable Chemistry & Engineering*, *6*(8), 10896–10904. https://doi.org/10.1021/acssuschemeng.8b02186

Zhang, G., He, Y., Wang, H., Feng, Y., Xie, W., & Zhu, X. (2019). Application of mechanical

crushing combined with pyrolysis-enhanced flotation technology to recover graphite and LiCoO2 from spent lithium-ion batteries. *Journal of Cleaner Production*, *231*, 1418–1427. https://doi.org/https://doi.org/10.1016/j.jclepro.2019.04.279

Zhang, G., Liu, Z., Yuan, X., He, Y., Wei, N., Wang, H., & Zhang, B. (2022). Recycling of valuable metals from spent cathode material by organic pyrolysis combined with in-situ thermal reduction. *Journal of Hazardous Materials*, *430*, 128374. https://doi.org/https://doi.org/10.1016/j.jhazmat.2022.128374

Zieminski, S. A., & Whittemore, R. C. (1971). Behavior of gas bubbles in aqueous electrolyte solutions. *Chemical Engineering Science*, *26*(4), 509–520. https://doi.org/https://doi.org/10.1016/0009-2509(71)83031-2

Trittin, J. 2004. Promulgation of the New Version of the Ordinance on Requirements for the Discharge of Waste Water into Waters (Waste Water Ordinance - AbwV) of 17. June 2004. Accessed on March 1, 2021 at https://www.bmuv.de/fileadmin/bmu-import/files/pdfs/allgemein/application/pdf/wastewater_ordinance.pdf.

Supplementary material

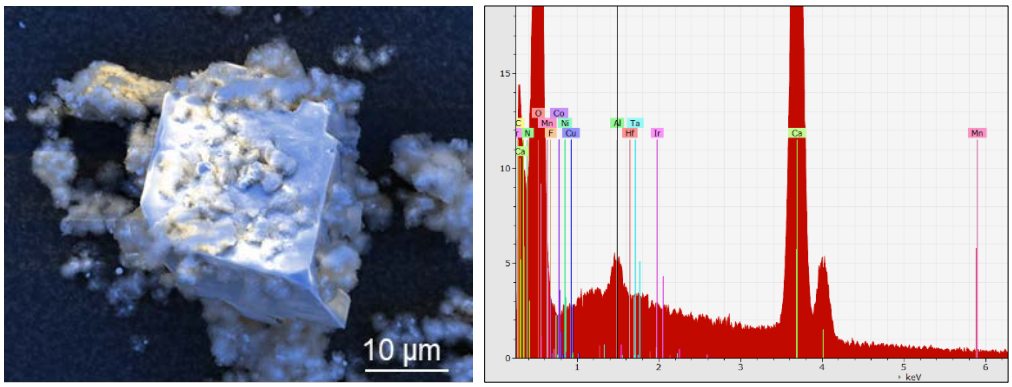

Figure S1. Calcium-rich particle observed through SEM imaging and its EDS spectrum.